Original Article

Synthesis and *in vivo* evaluation of an ^{18}F-labeled glycoconjugate of PD156707 for imaging ET$_A$ receptor expression in thyroid carcinoma by positron emission tomography

Simone Maschauer[1], Kristin Michel[2], Philipp Tripal[1], Katrin Büther[2], Torsten Kuwert[1], Otmar Schober[2], Klaus Kopka[2]*, Burkhard Riemann[2], Olaf Prante[1]

[1]Department of Nuclear Medicine, Laboratory of Molecular Imaging and Radiochemistry, Friedrich-Alexander University, 91054 Erlangen, Germany; [2]Department of Nuclear Medicine, University Hospital Münster, 48149 Münster, Germany; *New address: Radiopharmaceutical Chemistry, German Cancer Research Center (dkfz), 69120 Heidelberg, Germany

Abstract: Disturbances of the endothelin axis have been described in tumor angiogenesis and in highly vascularized tumors, such as thyroid carcinoma. Consequently, the endothelin (ET) receptor offers a molecular target for the visualization of the endothelin system *in vivo* by positron emission tomography (PET). We therefore endeavoured to develop a subtype-selective ET$_A$ receptor (ET$_A$R) radioligand by introduction of a glycosyl moiety as a hydrophilic building block into the lead compound PD156707. Employing click chemistry we synthesized the triazolyl conjugated fluoroglucosyl derivative **1** that had high selectivity for ET$_A$R (4.5 nM) over ET$_B$R (1.2 µM). The radiosynthesis of the glycoconjugate [^{18}F]**1** was achieved by concomitant ^{18}F-labeling and glycosylation, providing [^{18}F]**1** in high radiochemical yields (20-25%, not corrected for decay, 70 min) and a specific activity of 41-138 GBq/µmol. Binding properties of [^{18}F]**1** were evaluated *in vitro*, and its biodistribution was measured in K1 thyroid carcinoma xenograft nude mice *ex vivo* and by molecular imaging. Although the very substantial excretion via hepatobiliary clearance was not decisively influenced by glycosylation, the ^{18}F-glycoconjugate was more stable in blood during PET recordings than was the previously described ^{18}F-fluoroethoxy analog. Small-animal PET imaging showed displacable binding of [^{18}F]**1** at ET$_A$R in K1 tumors. The simple and efficient ^{18}F-radiosynthesis together with the excellent stability make the ^{18}F-labeled glycoconjugate [^{18}F]**1** a promising molecular tool for preclinical PET imaging studies of ET$_A$R expression in thyroid carcinoma and other conditions with marked angiogenesis.

Keywords: Endothelin receptor, angiogenesis, positron emission tomography (PET), ^{18}F, glycosylation, thyroid carcinoma

Introduction

Papillary (PTC) and follicular (FTC) thyroid carcinomas together constitute differentiated thyroid carcinoma (DTC), which is the most common endocrine malignancy. The incidence of DCT has risen steeply in the past three decades [1], not totally attributable to increased detection [2]. Since these carcinomas grow slowly and are generally well-treated by surgical resection and postoperative radioiodide ablation with iodide-131, 80-90% of patients suffering from DTCs survive longer than 10 years [3]. Nevertheless, a significant number of DTCs eventually become unresponsive to radioiodide treatment [4]. Since thyroid tissue is highly vascularized [5] combination therapy with anti-angiogenic agents is potentially beneficial for these patients [6]. Indeed, DTCs are responsive to inhibitors of tyrosine kinase receptors of vascular endothelial growth factor (VEGF-R), and other tyrosine kinase receptors such as EGFR (Vandetanib; [7]), PDGFR (Axitinib; [8]) or KIT (Motesanib; [9]).

In addition to VEGF and its receptors, the so-called endothelin axis is involved in tumor growth and progression [10]. The endothelin
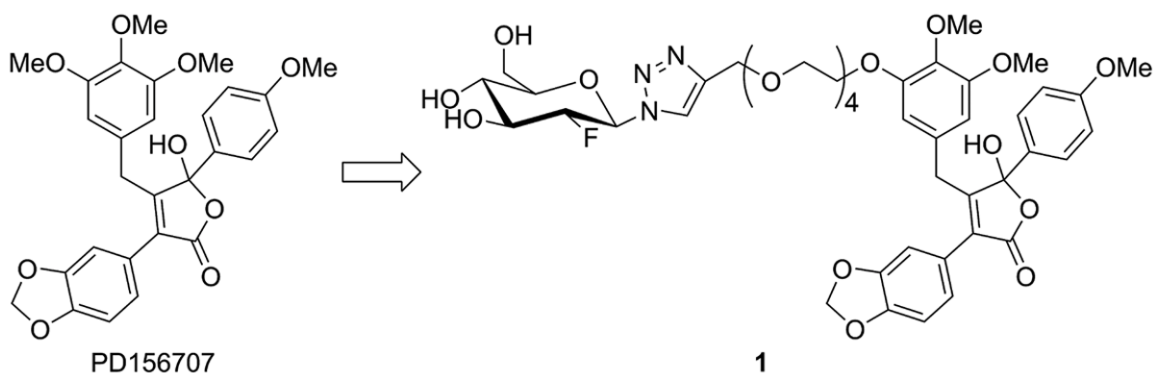
Figure 1. Chemical structure of PD156707 as lead compound and glycosylated analog **1**.

axis consists of the vasoactive peptide endothelin (ET) [11, 12], which occurs in three isoforms (ET-1, ET-2, and ET-3), along with two distinct receptor subtypes (ET$_A$R and ET$_B$R) [13-15]. Activation of ET$_A$R by ET-1 contributes to the progress of angiogenesis through stimulation of VEGF expression [10, 16]. Since increased expression of the ET axis is reported in DTCs [17-19], the ET$_A$R is a potential target for molecular imaging by positron emission tomography (PET), with an aim to improved clinical diagnosis and the prediction of therapy response. To this end, we have developed ^{18}F-labeled derivatives of the non-peptide ET$_A$R ligand PD 156707, such as a fluoroethoxy derivative [20, 21]. However, these compounds suffered from an unfavourable biodistribution due to their high lipophilicity. Drawing upon our previous experience with click-chemistry of ^{18}F-labeled carbohydrates [22, 23], we now report an optimized radiosynthesis of a subtype-selective ET$_A$R radioligand with introduction of a glycosyl moiety as a radiolabeled hydrophilic building block into the lead structure (**Figure 1**). We tested the hypothesis that this approach should impart improved pharmacokinetics of the ^{18}F-labeled ET$_A$R ligand by undertaking biodistribution studies and small animal PET imaging of ET$_A$R expression in living mice bearing ET$_A$R-positive papillary thyroid K1 tumors.

Materials and methods

General

^{1}H and ^{13}C NMR spectra were recorded on a Bruker AV400 spectrometer. Mass spectrometry analysis (ESI-EM) was performed using a MicroTOF (Bruker Daltronics, Bremen) instrument. Thin layer chromatography (TLC) was carried out on silica gel-coated polyester-backed TLC plates (Polygram, SIL G/UV$_{254}$, Macherey-Nagel) using solvent mixtures of methanol (MeOH) and ethyl acetate (EtOAc). Compounds were visualized by UV light (254 nm). HPLC was performed using a Knauer K-1800 pump, and S-2500 UV detector (Herbert Knauer GmbH, Berlin, Germany), with data processing by the ChromGate HPLC software (Knauer). The purity of all biologically tested and radioactive compounds was confirmed by RP-HPLC; unless otherwise state, we used a Nucleosil 100-5 analytical column (C18, 250 × 4.6 mm) with initial isocratic flow at 1.5 mL/min for 4 minutes of 40% CH$_3$CN in water (0.1% TFA), followed by a linear gradient to 95% CH$_3$CN in water (0.1% TFA) over 31 minutes.

Synthesis of the glycoconjugate 1

A solution of copper(II)sulfate pentahydrate (0.4 M, 0.18 mL) and sodium ascorbate (0.6 M, 0.12 mL) was added to a solution of 2-deoxy-2-fluoro-β-D-glucopyranosyl azide [23] (0.12 g, 0.6 mmol) and the alkyne-containing compound **2** (21) (0.35 g, 0.5 mmol) in EtOH (5 mL). The mixture was stirred at room temperature overnight. The solvent was evaporated *in vacuo* and the residue was redissolved in H$_2$O and CHCl$_3$. The aqueous layer was extracted with CHCl$_3$ (3 × 5 mL), and the combined organic phases were dried (MgSO$_4$). After evaporation of the solvent, the residue was purified by silica gel column chromatography to afford **1** as a pale yellow solid (0.31 g, 0.34 mmol, 57%). TLC (EtOAc:MeOH, 9:1): R$_f$ = 0.19. ^{1}H NMR (400 MHz, DMSO-d6) δppm 8.48 (s, 1H), 8.15 (s, br, 1H), 7.41-7.34 (m, 2H), 6.97-6.85 (m, 5H), 6.09-

5.90 (m, 5H), 5.82 (d, ^3J = 5.3 Hz, 1H), 5.48 (d, ^3J = 5.7 Hz, 1H), 4.85 (dt, ^2J = 50.9 Hz, ^3J = 9.0 Hz, 1H), 4.74 (t, ^3J = 5.9 Hz, 1H), 4.54 (s, 2H), 3.80-3.24 (m, 32H). ^{13}C NMR (101 MHz, DMSO) δ/ppm 170.7, 161.4, 159.6, 152.2, 151.3, 147.3, 146.9, 144.5, 135.9, 131.6, 129.0, 127.6, 126.6, 123.4, 123.3, 123.0, 113.6, 109.3, 108.1, 107.2, 106.3, 105.8, 101.2, 90.8 (d, J = 186 Hz), 84.0 (d, J = 24 Hz), 79.9, 74.4, 74.3, 69.9, 69.8, 69.7, 69.4, 69.3, 69.2, 68.8, 67.8, 63.3, 60.4, 59.8, 55.4, 55.1, 31.3, 31.3. ^{19}F NMR (DMSO-d6) δ/ppm -198.4. MS-EI-EM m/e = 936.3174 ((M + Na)$^+$) calcd for $C_{44}H_{52}FN_3O_{17}$Na 936.3173. HPLC t_R = 15.4 ± 0.2 min (95.1%).

Determination of receptor affinities

Microsomes were prepared by homogenizing myocardial ventricles from CD1 nude mice at 4°C for 90 s in 1 mL of buffer A (10 mM EDTA, 10 mM HEPES, 0.1 mM benzamidine, pH 7.4), using a Polytron PT 1200 (Kinematica, Lucerne, Switzerland). Homogenates were centrifuged at 45,000 g for 15 min at 4°C. The pellets were resuspended in 1.8 mL of buffer B (1 mM EDTA, 10 mM HEPES, 0.1 mM benzamidine, pH 7.4) and recentrifuged at 45,000 g for 15 min at 4°C. The second pellets were resuspended in 1.8 mL of buffer B and centrifuged at 10,000 g for 10 min at 4°C. The supernatants were recentrifuged at 45,000 g for 15 min at 4°C. The final pellets, consisting of partially enriched membranes, were resuspended in buffer C (50 mM Tris-HCl, 5 mM MgCl$_2$, pH 7.4), and stored frozen at -80°C. For competition binding studies, the prepared membranes were resuspended in buffer D (10 mM Tris-HCl, 154 mM NaCl, 10 mM MgCl$_2$, 0.3% BSA pH 7.4) at 0°C. Portions of suspensions containing 10 μg of membranes were incubated with a constant concentration of [^{125}I]ET-1 (40 pM, Perkin-Elmer Live Sciences Inc., Billerica, MA, USA) and with varying concentrations (1 pM-10 μM) of **1** at 37°C for 2 h, followed by rapid filtration on Whatman GF/B filters and washing with ice-cold distilled water. The membrane bound radioactivity was determined in a γ-scintillation counter. Competition binding curves were analyzed by nonlinear regression analysis using the XMGRACE program (Linux software). The high- and low-affinity IC$_{50}$ values were converted into the high- and low-affinity inhibition constants (K_i(ET$_A$R) and K_i(ET$_B$R)) by the method of Cheng-

Prusoff [24] using the previously determined K$_d$ value of [^{125}I]ET-1 [20].

Production of [^{18}F]fluoride

No-carrier-added (n.c.a.) [^{18}F]fluoride was produced by the ^{18}O(p,n)^{18}F reaction in ^{18}O-enriched (97%) water using a proton beam of 11 MeV generated by a RDS 111e cyclotron (CTI-Siemens) and trapped on an anion exchange cartridge (QMA, Waters).

Radiosynthesis of [^{18}F]1

The QMA-cartridge with [^{18}F]fluoride (400-700 MBq; PET Net GmbH, Erlangen) was eluted with a solution of Kryptofix® 2.2.2 (10 mg), K$_2$CO$_3$ (0.1 M, 15 μL) and KH$_2$PO$_4$ (0.1 M, 18 μL) in acetonitrile/water (8:2, 1 mL). The water was removed by evaporation to dryness with acetonitrile (3 × 200 μL) using a stream of nitrogen at 85°C. The precursor 3,4,6-tri-O-acetyl-2-O-trifluoromethanesulfonyl-β-D-mannopyranosyl azide **3** (23) (9 mg, 15 μmol) in anhydrous acetonitrile (450 μL) was added to the dried K$^+$/Kryptofix 2.2.2/^{18}F-complex and the solution was stirred for 2.5 min at 85°C. The solvent was evaporated, the residue was redissolved in acetonitrile (0.1% TFA)/water (0.1% TFA) 30:70 (500 μL), and 3,4,6-tri-O-acetyl-2-deoxy-2-[^{18}F]fluoroglucopyranosyl azide **[^{18}F]4** was isolated by semipreparative HPLC (Kromasil C8, 125 × 8, 4 mL/min, 30-70% acetonitrile (0.1% TFA) in water (0.1% TFA) in a linear gradient over 30 min, t_R = 10 min) and trapped on a C18 cartridge (Lichrosorb, Merck, 100 mg). After elution with ethanol (0.8 mL) and evaporation of the solvent, a solution of NaOH (10% ethanol, 60 mM NaOH, 250 μL) was added. After 5 min at 60°C (formation of 2-deoxy-2-[^{18}F]fluoroglucopyranosyl azide), HCl (0.1 M, 10 μL) was added to neutralize the solution, followed by a solution of alkyne-functionalized **2** (300 nmol) dissolved in 200 μL ethanol, sodium ascorbate (0.6 M, 10 μL), and CuSO$_4$ (0.2 M, 10 μL). After the reaction mixture had been stirred for 15 min at 60°C, [^{18}F]1 was isolated by semipreparative HPLC (Kromasil C8, 125 × 8, 4 mL/min, 30-70% acetonitrile (0.1% TFA) in water (0.1% TFA) in a linear gradient over 30 min, t_R = 9 min) and subsequent SPE (solid phase extraction, Lichrosorb, Merck, 100 mg). [^{18}F]1 (80-150 MBq) was eluted from the cartridge with 1 ml ethanol, the solvent was evaporated in vacuo and the residue was dissolved in PBS (pH 7.4)

for *in vitro* and *in vivo* use. The [18F]-labeled **1** was identified by retention time (t$_R$) by means of the radio-HPLC system and by co-injection of the corresponding reference compound. Kromasil C8, 250 × 4.6 mm, 40-100% acetonitrile (0.1% TFA) in water (0.1% TFA) in a linear gradient over 50 min, 1.5 mL/min, t$_R$ = 6.3 min. The overall radiochemical yield was 20-25% (not corrected for decay, referred to used [18F]fluoride) in a total synthesis time of 70 min.

Determination of tracer stability in human serum

An aliquot of [**18F**]**1** in PBS (40 μL, pH 7.4) was added to human serum (200 μL) and incubated at 37°C. Aliquots (40 μL) were taken at various time intervals (5, 15, 30, 60, 90 min) and proteins were precipitated by addition of methanol/CH_2Cl_2 (1:1, 100 μL). The samples were centrifuged, and the supernatants were analyzed by radio-HPLC (Kromasil C8, 250 × 4.6 mm, 40-100% acetonitrile (0.1% TFA) in water (0.1% TFA) in a linear gradient over 50 min, 1.5 mL/min, t$_R$ = 6.3 ± 0.2 min).

Determination of distribution coefficient at pH 7.4 (logD$_{7.4}$)

The partition ratio of [**18F**]**1** between water and 1-octanol was determined as the distribution coefficient at pH 7.4. 1-Octanol (0.5 mL) was added to a solution of [**18F**]**1** in PBS (0.5 mL, 25 kBq, pH 7.4) and the layers were vigorously mixed for 3 min at room temperature. The tubes were centrifuged (17,000 g, 1 min) and three samples of 100 μL of each layer were counted in a γ-counter (Wallac Wizard). The distribution coefficient was determined by calculating the ratio cpm (1-octanol)/cpm (PBS) and expressed as logD$_{7.4}$ (log(cpm$_{1-octanol}$/cpm$_{buffer}$)). Two independent experiments were performed in triplicate. Data are reported as mean ± SD.

Cell culture

The human ET$_A$R expressing cell line K1 was purchased from the European Collection of Cell Cultures (ECACC, N° 92030501) and grown in culture medium (DMEM with L-glutamine/ Kaighn's F-12 Nutrient Mixture (1:1)) supplemented with 10% fetal bovine serum (FBS) at 37°C in a humidified atmosphere of 5% CO_2. Cells were routinely subcultured every 3-4 days. The cells were routinely tested for con-

tamination with mycoplasma and tests were always negative.

Saturation binding studies using K1 cells

Approximately 100,000 K1 cells were seeded in 24-multiwell plates 24 h before experimental use. The medium was changed to 0.5 mL binding buffer (culture medium supplemented with 1% bovine serum albumin (BSA)), and **1** containing [**18F**]**1** (25 kBq) was added to each well over a range of final ligand concentrations between 0.2 nM and 100 nM for the determination of total binding. For the determination of nonspecific binding, tracer was added in the same concentrations as aforementioned but cells were preincubated (10 min, 37°C) with PD156707 to a final concentration of 5 μM. After incubation for 60 min at 37°C, the cells were placed on ice and washed rapidly twice with ice-cold PBS. Cells were lysed with NaOH (0.1 M, 1 mL) and counted in a γ-counter (Wallac 1470 Wizard®, Perkin Elmer). After homogenization of the samples by short ultrasonic pulses, protein concentration was measured by the method of Bradford (25). This experiment was performed twice in quadruplicate. B$_{max}$ and K$_d$ values were calculated using the software GraphPad Prism.

Preparation of cell lysates

For preparation of protein extracts, the cells were lysed in RIPA buffer (50 mM Tris/HCl, pH 7.5, 150 mM NaCl, 1% IGEPAL CA-630, 0.5% sodium deoxycholate, 0.1% SDS, all obtained from Sigma-Aldrich (St. Louis, USA)), and complete protease inhibitor tablets from Roche (Mannheim, Germany). Lysis was performed for 10 min on ice. Subsequently, cellular debris was removed by centrifugation (25,000 g, 10 min, 4°C). The protein concentration within cell extracts was determined using the BCA assay kit (Sigma-Aldrich) according to the manufacturer's instructions.

Preparation of tissue lysates

For preparation of protein extracts from xenograft tumor tissue, the tumor bearing mice were killed by cervical dislocation, and the tissue was removed and subsequently frozen in an isopropyl alcohol/dry ice bath (-86°C) and stored at -80°C. Thin sections (50 μm) of the tissue were lysed in RIPA buffer with addition of

complete protease inhibitor tablets for 30 min on ice. The tissue thin sections were then homogenized by three short ultrasonic pulses (0.4 sec, 7 W, Bandelin Sonoplus, HD2070). After lysis, tissue debris was removed by centrifugation (25,000 g, 10 min, 4°C), and the protein concentration within suspended tissue extracts was determined by the BCA assay kit (Sigma-Aldrich) according to the manufacturer's instructions.

Western blot analysis

Lysate samples with a total protein content of 10 μg were separated by 10% sodium dodecyl-sulfate-polyacrylamide gel electrophoresis and transferred to a PVDF-membrane (GE Healthcare, Chalfont St Giles, UK) at 15 V for 25 min. Blots were incubated in 2.5% milk powder (Roth, Karlsruhe, Germany) and 0.1% Tween 20 (Roth) in PBS (Sigma-Aldrich) overnight at 4°C. After washing in PBS/0.1% Tween 20 for 15 min, blots were incubated for one hour at room temperature with primary polyclonal endothelin receptor-A antibody derived from rabbit (1:200; Santa Cruz, Santa Cruz, USA), and for 1 hour with primary glyceraldehyde-3-phosphate dehydrogenase (GAPDH) antibody from mouse (1:2.000; Millipore, Billerica, USA). After washing in PBS/0.1% Tween 20 three times, blots were incubated for one hour at room temperature with the secondary antibodies goat anti-rabbit IgG (1:10000; Calbiochem, Darmstadt, Germany) and goat anti-mouse IgG (1:20000; Calbiochem), both coupled to horseradish peroxidase. All antibodies were diluted in 0.5% milk powder solution and 0.1% Tween 20 in PBS. The visualization of bound antibody was performed using the enhanced chemoluminescence Western blotting detection system (ECL, GE Healthcare, Chalfont St Giles, UK) and a high-sensitivity camera device (FluorSMax, Bio-Rad, Munich, Germany).

Immunofluorescence analysis

Thin sections (10 μm) of cryopreserved xenograft tissue were fixed in acetone at -20°C for 90 s, and washed three times for one minute in PBS. To decrease nonspecific binding of the secondary antibody, tissue thin sections were blocked for 10 min in PBS containing 10% normal goat serum. For detection of the murine endothelial cell antigen (MECA32), tissue thin sections were incubated with an anti-MECA32

antibody (a kind gift from Dr. Christoph Daniel, Department of Nephropathology, University Hospital Erlangen) diluted 1:3 in PBS, 10% normal goat serum (Dako, Glostrup, Denmark) and to detect the human endothelin receptor-A (ET$_A$R), the anti-ET$_A$R-antibody (Santa Cruz, Santa Cruz, USA) was used at a dilution of 1:100. After washing (3 × 5 min in PBS), the incubation continued with a Cy3-conjugated goat anti-rat IgG (Jackson, West Grove, USA), diluted 1:500 in PBS (containing 10% normal goat serum) to detect the anti-MECA32 antibody. A fluorescein-conjugated anti-rabbit IgG (Calbiochem) at a dilution of 1:100 in PBS (containing 10% normal goat serum) was used to visualize the binding of the anti-ET$_A$R-antibody. The negligible nonspecific binding of all secondary antibodies under the experimantal conditions described above was successfully vefified by staining experiments in which the primary antibody was omitted. The fluorescence images were captured using a fluorescence microscope (EVOS, AMG, Bothell, USA).

Tumor model

All animal experiments were performed in compliance with the protocols approved by the local Animal Protection Authorities (Regierung Mittelfranken, Ansbach, Germany, No. 54-2532.1-15/08). Athymic nude mice (nu/nu) were obtained from Harlan Winkelmann GmbH (Borchen, Germany) at 10-12 weeks of age and were kept under standard conditions (12 h light/dark) with food and water available ad libitum. K1 cells were harvested and suspended in sterile PBS at a concentration of 2.5×10^7 cells/mL, respectively. Viable cells (5×10^6) in PBS (200 μL) were injected subcutaneously into the back. Two to three weeks after inoculation (tumor weight: 50-100 mg), the mice (about 12-15 weeks old with about 40 g body weight) were used for biodistribution and small-animal PET studies.

Determination of metabolic stability of [^{18}F]1

Nude mice (n = 3) bearing K1 tumors were injected with 6-8 MBq of [^{18}F]**1** via a tail vein. At 60 min after tracer injection the animals were killed by cervical dislocation and dissected. Blood, duodenum and gall bladder were collected. Blood was immediately centrifuged for 5 min at 17,000 g. Tissue and plasma samples were cooled to < 0°C, 200 μL of 10% acetoni-
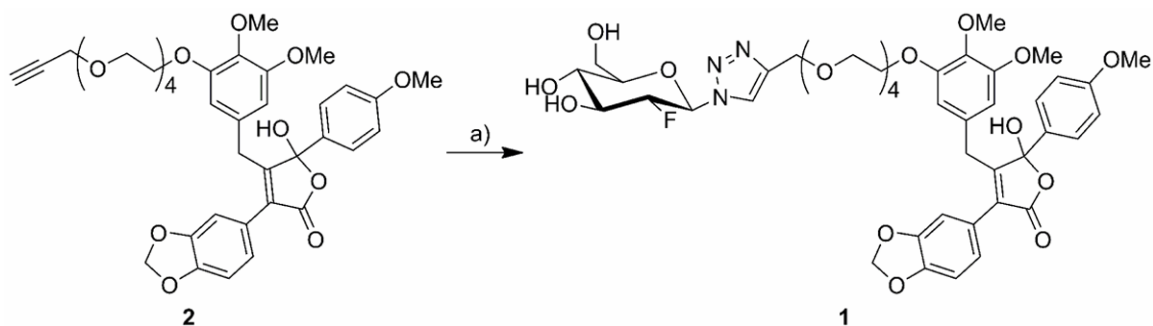
Figure 2. Scheme of the synthesis of glycosylated reference compound **1**. Reaction conditions: a) 2-deoxy-2-fluoro-β-D-glucopyranosyl azide, CuSO$_4$ (14 mM), sodium ascorbate (21 mM), EtOH, overnight, rt.

Table 1. Receptor binding affinities (K$_i$ values) of **1** for ET$_A$R and ET$_B$R in comparison with lead compound PD156707[a]
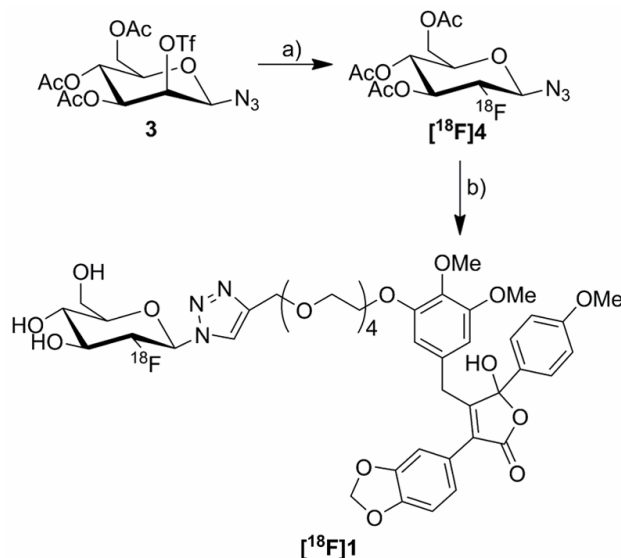
Compound	ET$_A$R	ET$_B$R
PD156707	0.17 nM[b]	133.8 nM[b]
1	4.5 ± 0.8 nM	1.2 ± 1.8 µM

[a]Values are given as mean ± standard deviation from three independent experiments. [b]Values from Reynolds et al. [27].

Figure 3. Radiosynthesis of [^{18}F]**1**. Reaction conditions: a) [^{18}F]F$^-$, 10 mg Kryptofix® 2.2.2, 1.75 µmol K$_2$CO$_3$, 1.75 µmol KH$_2$PO$_4$, acetonitrile (400 µL), 2 min, 85°C [23], b) 1. NaOH (60 mM), 5 min, 60°C; 2. addition of HCl (1 M, 10 µL), **2** (0.2 mg, 0.3 µmol), sodium ascorbate (0.6 M, 10 µL), CuSO$_4$ (0.2 M, 10 µL), PBS/EtOH (1:1), V = 500 µL, 15 min, 60°C.

trile (0.1% TFA) was added, and the mixtures were homogenized at < 0°C using a Bandelin Sonopuls. The samples were centrifuged for 5 min at 17,000 g, and the supernatants were analyzed by radio-HPLC (Kromasil C8, 250 × 4.6 mm, 40-100% acetonitrile (0.1% TFA) in water (0.1% TFA) in a linear gradient over 50 min, 1.5 mL/min).

Biodistribution studies

[^{18}F]**1** (5-10 MBq/mouse) was intravenously injected into K1 xenografted mice (n = 3) via a tail vein. Mice were killed by cervical dislocation at 10, 30 and 60 min post-injection (p.i.). Tumors and other tissues (blood, lung, liver, kidneys, heart, spleen, muscle, stomach, gall bladder, duodenum and intestine) were dissected and weighed. Radioactivity concentration of the dissected tissues was determined using a γ-counter (Wallac 1470 Wizard®, Perkin Elmer), corrected to time of injection, and reported as percentage of injected dose per gram of tissue (%ID/g), for calculation of tumor-to-organ ratios. Blocking experiments were carried out in randomly chosen mice (n = 3) by co-injecting 25 µg PD156707 (625 µg/kg body weight) together with the radiotracer; these mice were killed by cervical dislocation at 60 min p.i., and tissue radioactivities measured as above.

Small-animal PET imaging

PET scans and image analysis were performed using a small-animal PET rodent model scanner (Inveon, Siemens Medical Solutions). Mice (n = 5) were anaesthized with isoflurane (4%) and placed in the aperture of the tomograph. Upon intravenous injection of 3-10 MBq [^{18}F]**1** to a tail vein, acquisition of a 60 min dynamic scan was initiated (12 × 10 sec, 3 × 1 min, 5 × 5 min, 3 × 10 min,
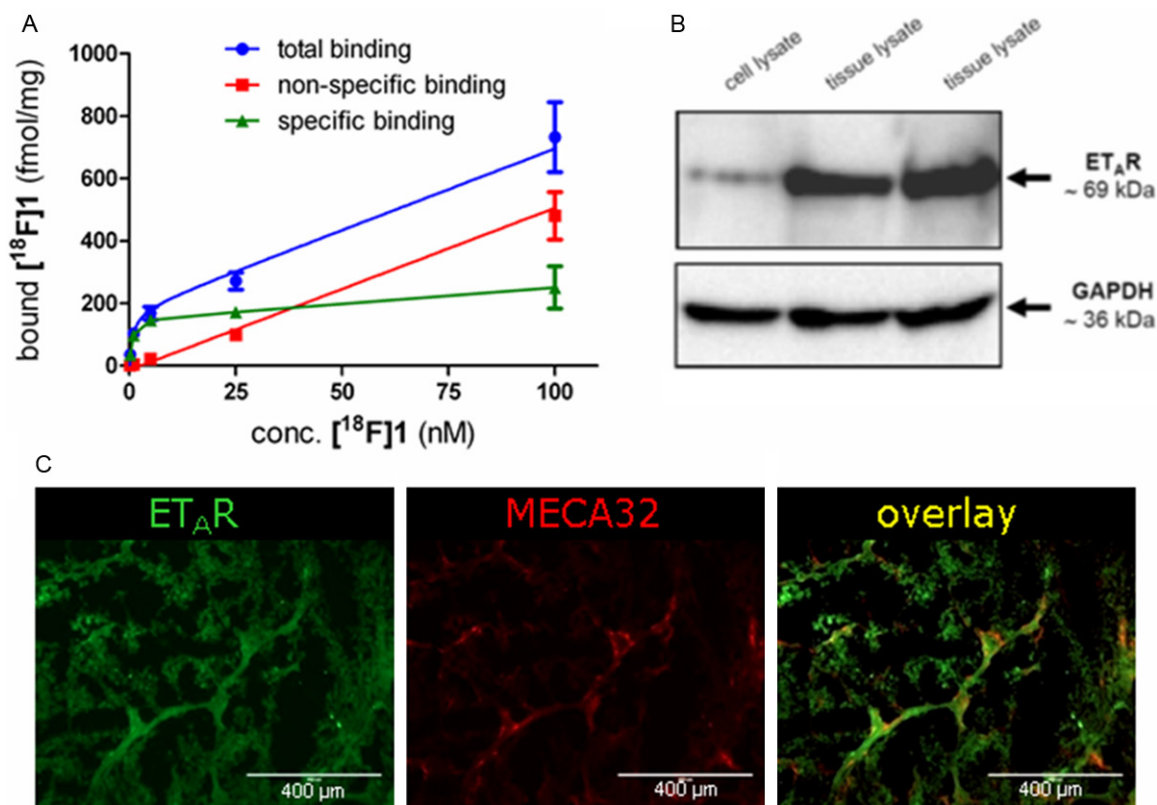
Figure 4. A: Saturation binding curve of [^{18}F]**1** to ET$_A$ receptors on K1 cells *in vitro*. Data are expressed as mean (± SD) (n = 4). B: ET$_A$R is expressed in K1 cells and in K1 xenograft tissue. Cells or tissue slices (50 μm) were lysed and samples with equal protein content were separated by polyacrylamide gel electrophoresis; ET$_A$R and GAPDH were then quantified by Western blot analysis, with Magic Mark® (Invitrogen) serving as a molecular weight marker. The band at 69 kDa represents the ET$_A$R and the band at 36 kDa the GAPDH protein. ET$_A$R expression is clearly present in tissue lysates from K1 xenograft tumors tissue (lane 2, lane 3: two independent samples), whereas ET$_A$R expression is lower in lysates derived from K1 cells (lane 1). Corresponding GAPDH signals confirm equal protein loading. C: ET$_A$R is expressed in K1-xenograft tissue and murine tumor vessels. Xenograft K1 tumor tissue was dissected from nude mice and subsequently cryopreserved. Thin sections of K1 tumor tissue were co-stained for ET$_A$R (green) and the murine endothelial cell antigen MECA32 (red). Immunofluorescence of ET$_A$R was excited at 470 nm and emitted at 525 nm. MECA32 fluorescence was excited at 530 nm and emitted at 593 nm. Images were captured at a magnification of 10-fold and the bar displayed corresponds to a distance of 400 μm.

total of 23 frames). After 3D-OSEM iterative image reconstruction with decay and attenuation correction, regions of interest (ROIs) were drawn over the tumor region, and the mean within a tumor was converted to uptake values (%ID/g). For receptor-blocking experiments, nude mice (n = 4) bearing K1 tumors were scanned as described above after coinjection with [^{18}F]**1** (3-10 MBq) and PD156707 (25 μg/animal).

Results and discussion

Starting from the alkyne precursor **2**, which has been described previously [21], the synthesis of the glycoconjugate **1** was performed by click chemistry with applying the copper(I)-catalyzed azide alkyne 1,3-dipolar cycloaddition (CuAAC) in the presence of 2-deoxy-2-fluoro-β-D-glucopyranosyl azide [23], sodium ascorbate and CuSO$_4$ (**Figure 2**). After confirmation of identity and purity of title compound **1**, competition binding studies were carried out for the endothelin receptor subtypes ET$_A$R and ET$_B$R using [^{125}I]ET-1 and membranes from mouse myocardial ventricles, as described previously [21]. We found that **1** inhibited [^{125}I]ET-1 binding at ET$_A$R with a K$_i$ value of 4.5 nM, whereas inhibition at ET$_B$R required a 266-fold higher concentration (**Table 1**). This ET$_A$R/ET$_B$R subtype selectivity of **1** is three times lower than that of the ET$_A$R-selective reference ligand PD 156707.
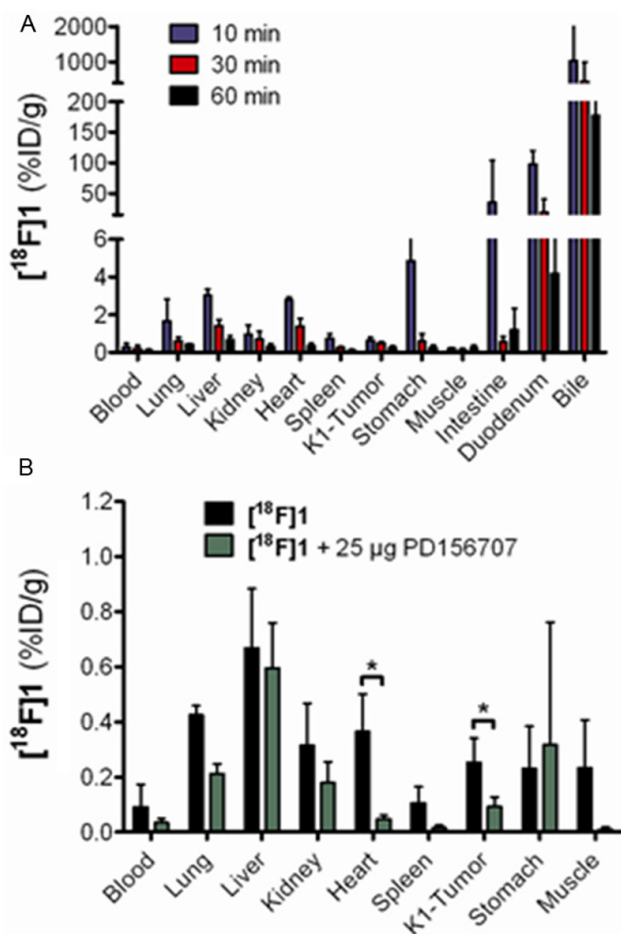
Figure 5. A: Biodistribution of [^{18}F]**1** in K1 xenografted nude mice at 10, 30 and 60 min p.i. and (B) Biodistribution of [^{18}F]**1** coinjected with PD156707 (25 µg/animal) at 60 min p.i. Data are expressed as mean (± SD) of determinations in three animals. The asterisk indicates significant differences ($P < 0.05$, t-test) between coinjected and control animals for the tracer uptake in heart and K1 tumor tissue.

Therefore, glycosylation of **2** resulted in some loss of ET$_A$R subtype selectivity for glycosyl derivative **1**, although this reduced selectivity is unlikely to be physiologically relevant. This result confirmed our previous study of a series of fluorinated derivatives of the ET$_A$R antagonist PD 156707 [21], indicating very similar receptor binding data for ET$_A$R affinity and subtype selectivity.

Encouraged by the favorable *in vitro* binding results, we proceeded to set up and optimize the radiosynthesis of ^{18}F-labeled **1**, and characterize its binding properties *in vivo* binding properties using nude mice bearing ET$_A$R-positive thyroid K1 tumors. As shown in **Figure 3**, the radiosynthesis of [^{18}F]**1** accomplished

through concomitant ^{18}F-labeling and glycosylation [22]. In general, this strategy followed the previously described concept for the fluoroglycosylation of peptides, although obtain an optimized radiochemical yield (RCY) entailed some modifications. In particular, the amount of precursor was increased from 100 nmol (sufficient for peptide labeling [22]) to 300 nmol of the alkyne-bearing precursor **2**, and the ethanol content of the solvent was increased from 10% to 60% to provide higher solubility of the non-peptidic precursor **2**.

Starting from triflate precursor **3** [23], 2-deoxy-2-[^{18}F]fluoroglucopyranosyl azide ([^{18}F]**4**; **Figure 3**) was produced in about 30 min, including the adjacent deacetylation under basic conditions. The subsequent CuAAC reaction in the presence of alkyne **2** (300 nmol) proceeded smoothly in a mixture of ethanol/PBS at 60°C, providing [^{18}F]**1** in a RCY of 70-75% after 15 min (**Figure 3**). In comparison with the ^{18}F-fluoroglucosylation of peptides [22], the amount of the alkyne precursor had thus to be increased threefold to achieve the optimum RCY. After semipreparative HPLC, [^{18}F]**1** was obtained in an overall radiochemical yield of 20-25% (not corrected for decay, referred to [^{18}F]fluoride) in a total synthesis time of 70 min. The specific activities of [^{18}F]**1** at end of preparation was in the range of 41-138 GBq/µmol. The chemical identity of [^{18}F]**1** and the high radiochemical purity (> 99%) were confirmed by HPLC. After formulation of an injectable solution of the radioligand, the stability of [^{18}F]**1** after incubation in human serum at 37°C was at least 99% (**Figure 6**).

To characterize the binding properties of [^{18}F]**1** *in vitro*, we performed saturation binding experiments with [^{18}F]**1** in a concentration range between 0.2 nM and 100 nM using the human papillary thyroid carcinoma cell line K1, which demonstrated ET$_A$R expression by Western Blot (**Figure 4A** and **4B**). Notably, the expression of ET$_A$R on K1 cells was rather low *in vitro*, compared to its expression in K1 tumor tissue (**Figure 4B**). **Figure 4A** demonstrated saturable specific binding of radioligand [^{18}F]**1** to K1 cells, indicating a dissociation constant (K_d) of 0.7 nM. We estimated the ET$_A$R density (B_{max}) to be
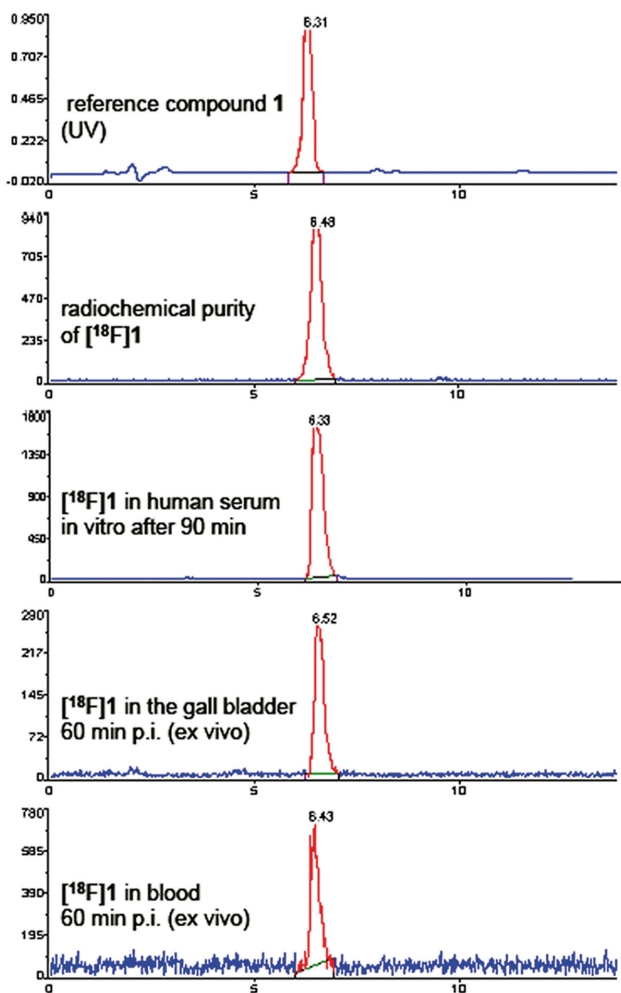
Figure 6. HPLC chromatograms showing the identity and radiochemical purity as well as the stability of [^{18}F]**1** in human serum *in vitro*, and in extracts from mouse blood and gall bladder collected at 60 min post-injection of the tracer (Kromasil C8, 250 × 4.6 mm, 40-100% acetonitrile (0.1% TFA) in water (0.1% TFA) in a linear gradient over 50 min, 1.5 mL/min).

191 fmol/mg, which represents only about 57,200 ET$_A$ receptors per K1 cell (191 fmol/mg = 9.5 × 10^{-5} fmol/cell = 57,200 receptors/cell). When analyzing the K1 tumor tissue derived from tumor-bearing nude mice, the overall expression of ET$_A$R was determined, which we ascribe to the endothelial cells in the highly vascularized K1 thyroid tumors. This association was demonstrated by co-staining for ET$_A$R and the murine endothelial cell antigen MECA32 in slices from K1 tumor tissue (**Figure 4C**).

The xenotransplantation of human thyroid K1 cells was performed by subcutaneous injection of a cell suspension of 5 million cells into nude mice, followed by growth of the tumors for about 14-20 days. The tumors then attained a diameter of 9-15 mm and showed only minor necrotic areas upon dissection. Our biodistribution study of [^{18}F]**1** in K1 xenografted nude mice at 10, 30, and 60 min post-injection (p.i.; **Figure 5**) revealed [^{18}F]**1** to have fast blood clearance, and low uptake in the kidneys and liver. In contrast, we observed very high uptake of the intact tracer as verified by HPLC in the bile and intestines (**Figures 5A**, **6**). This indicates predominant excretion of [^{18}F]**1** occurred via hepatobiliary clearance, a finding in accordance with previously studied ^{18}F-fluoroethoxy derivatives [20] and the PEGylated ^{18}F-derivatives of PD 156707 [21].

The present findings for biodistribution of glycosyl compound [^{18}F]**1** match closely with those described for ^{18}F-alkyl-labeled ET$_A$ radioligands [20, 21]. We recalculated the [^{18}F]**1** uptake values as an "uptake index" for direct comparison with corresponding results for the fluoroethoxy and other derivatives [20, 21]; this comparison revealed no major differences in the excretion pathway between the several tracers. The logD$_{7.4}$ value of the title compound (-0.4) indicates that glycosylation increased the hydrophilicity of the structure by a factor of 19, as compared to the most hydrophilic of the compounds reported in the paper by Michel *et al.*, which had a logD$_{7.4}$ of 0.89 [21]. This increased hydrophilicity did not markedly influence the biokinetics *in vivo*, and did not impair the hepatobiliary excretion. However, glycosylation of the lead structure PD156707 had greatly enhanced the metabolic stability of the tracer in blood of living mice. Whereas the fluoroethoxy derivative showed about 50% polar radiometabolites within 20 min after injection into mice [20], the glycosyl derivative [^{18}F]**1** was entirely stable in serum *in vitro* and likewise *in vivo*, as no radiometabolite was detected in blood or gall bladder at 60 min post-injection (**Figure 6**).

The uptake of [^{18}F]**1** in healthy myocardium and in K1 tumors was significantly higher in the unblocked condition than in animals co-injected with PD156707, providing evidence for specific ET$_A$R-mediated binding in these tissues *in vivo* (**Figure 5B**). The physiological specific bind-
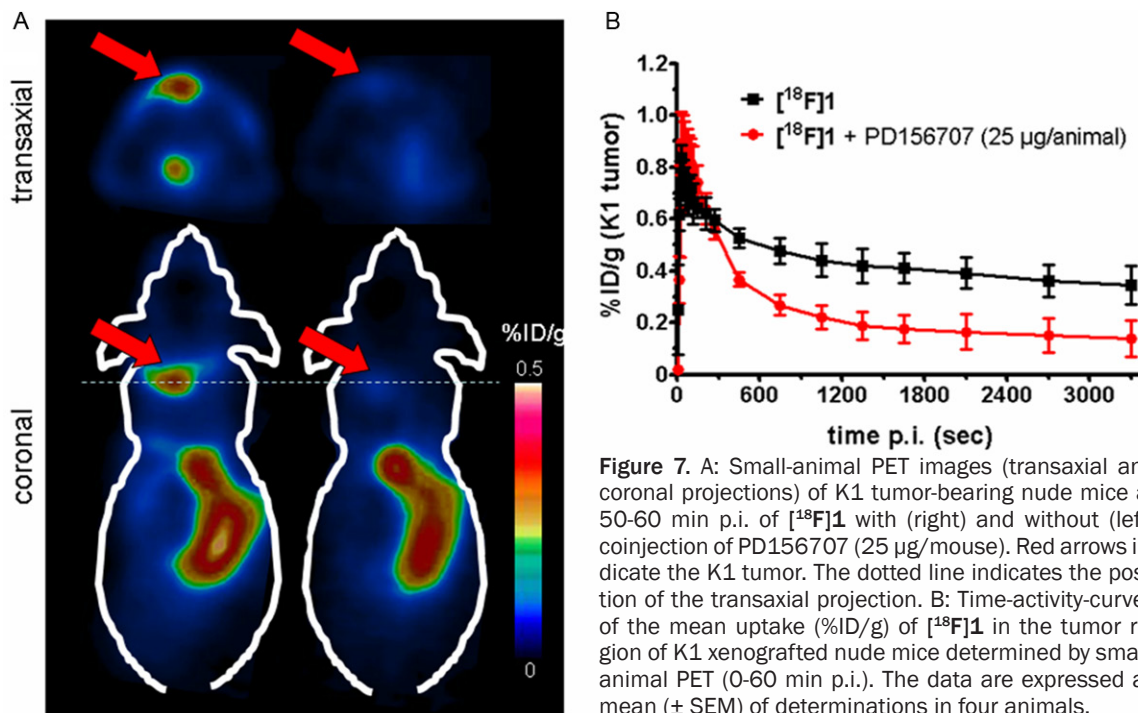
Figure 7. A: Small-animal PET images (transaxial and coronal projections) of K1 tumor-bearing nude mice at 50-60 min p.i. of [^{18}F]**1** with (right) and without (left) coinjection of PD156707 (25 μg/mouse). Red arrows indicate the K1 tumor. The dotted line indicates the position of the transaxial projection. B: Time-activity-curves of the mean uptake (%ID/g) of [^{18}F]**1** in the tumor region of K1 xenografted nude mice determined by small-animal PET (0-60 min p.i.). The data are expressed as mean (± SEM) of determinations in four animals.

ing in healthy myocardium suggests that this class of ligand might be a useful adjunct to ^{13}N-ammonia PET studies of endothelial function in heart [26]. The specific uptake of [^{18}F]**1** was 0.62 ± 0.18 %ID/g in tumor samples collected at 10 min, declining to about 0.25 ± 0.09 %ID/g at 60 min p.i. (**Figure 5A**). These findings ex vivo were entirely consistent with the time-activity curves derived from small-animal PET, which likewise revealed specific binding of [^{18}F]**1** in the tumor region, based on the more rapid clearance in animals coinjected with PD156707 (**Figure 7**). The mean uptake value (%ID/g) of [^{18}F]**1** by PET imaging at 55 min p.i. was 0.35 ± 0.07 (n = 4), declining to only 0.14 ± 0.07 (n = 4; ($P < 0.05$, t-test) in mice coinjected with PD156707), in close agreement with the dissection study (**Figure 5B**). Although the tumor uptake of [^{18}F]**1** and the tumor-to-tissue ratios were rather low, the ET$_A$R expression in K1 thyroid tumors was detectable by small-animal PET (**Figure 7A**); we are unaware of any previous molecular imaging studies of these thyroid tumors, so comparison of [^{18}F]**1** with other tracers is not possible. Given the excellent metabolic stability of [^{18}F]**1** *in vivo*, we find that [^{18}F]**1** PET has considerable potential for imaging ET$_A$R expression in thyroid tumors.

In conclusion, we established a reliable and efficient strategy of concomitant glycosylation and ^{18}F-labeling by click-chemistry of the ET$_A$R ligand PD156707, providing the ^{18}F-labeled glycoconjugate ligand [^{18}F]**1** for preliminary PET studies. As with the lead compound, the excretion of [^{18}F]**1** in mice occurred via hepatobiliary clearance and was not significantly influenced by glycosylation, which did however impart nearly complete metabolic stability *in vivo*. Biodistribution studies *ex vivo* and small-animal PET imaging proved the specificity of [^{18}F]**1** for ET$_A$R binding in K1 thyroid tumors and in healthy myocardium. However, [^{18}F]**1** revealed significant hydrophobicity with only low tumor uptake, rendering the clinical translation of this tracer highly unfavorable. Despite the apparently low expression of the marker in K1 thyroid xenografts, [^{18}F]**1** shows promise for studying ET$_A$R expression and its regulation in animal models of angiogenesis, notably in thyroid carcinoma.

Address correspondence to: Dr. Olaf Prante, Department of Nuclear Medicine, Laboratory of Molecular Imaging and Radiochemistry, Friedrich-Alexander University, Schwabachanlage 6, D-91054 Erlangen, Germany. Tel: +49 9131-8544440; Fax: +49 9131-8534440; E-mail: olaf.prante@uk-erlangen.de

References

[1] Zhu C, Zheng T, Kilfoy BA, Han X, Ma S, Ba Y, Bai Y, Wang R, Zhu Y, Zhang Y. A birth cohort analysis of the incidence of papillary thyroid cancer in the United States, 1973-2004. Thyroid 2009; 19: 1061-1066.

[2] Morris LG, Myssiorek D. Improved detection does not fully explain the rising incidence of well-differentiated thyroid cancer: a population-based analysis. Am J Surg 2010; 200: 454-461.

[3] Jossart GH, Clark OH. Well-differentiated thyroid cancer. Curr Probl Surg 1994; 31: 933-1012.

[4] Chougnet C, Brassard M, Leboulleux S, Baudin E, Schlumberger M. Molecular targeted therapies for patients with refractory thyroid cancer. Clin Oncol 2010; 22: 448-455.

[5] Fujita H, Murakami T. Scanning electron microscopy on the distribution of the minute blood vessels in the thyroid gland of the dog, rat and rhesus monkey. Arch Histol Jpn 1974; 36: 181-188.

[6] Keefe SM, Cohen MA, Brose MS. Targeting vascular endothelial growth factor receptor in thyroid cancer: the intracellular and extracellular implications. Clin Cancer Res 2010; 16: 778-783.

[7] Wells SA Jr, Gosnell JE, Gagel RF, Moley J, Pfister D, Sosa JA, Skinner M, Krebs A, Vasselli J, Schlumberger M. Vandetanib for the treatment of patients with locally advanced or metastatic hereditary medullary thyroid cancer. J Clin Oncol 2010; 28: 767-772.

[8] Cohen EE, Rosen LS, Vokes EE, Kies MS, Forastiere AA, Worden FP, Kane MA, Sherman E, Kim S, Bycott P, Tortorici M, Shalinsky DR, Liau KF, Cohen RB. Axitinib is an active treatment for all histologic subtypes of advanced thyroid cancer: results from a phase II study. J Clin Oncol 2008; 26: 4708-4713.

[9] Schlumberger MJ, Elisei R, Bastholt L, Wirth LJ, Martins RG, Locati LD, Jarzab B, Pacini F, Daumerie C, Droz JP, Eschenberg MJ, Sun YN, Juan T, Stepan DE, Sherman SI. Phase II study of safety and efficacy of motesanib in patients with progressive or symptomatic, advanced or metastatic medullary thyroid cancer. J Clin Oncol 2009; 27: 3794-3801.

[10] Bagnato A, Spinella F. Emerging role of endothelin-1 in tumor angiogenesis. Trends Endocrinol Metab 2003; 14: 44-50.

[11] Bagnato A, Rosano L. The endothelin axis in cancer. Int J Biochem Cell Biol 2008; 40: 1443-1451.

[12] Nelson J, Bagnato A, Battistini B, Nisen P. The endothelin axis: emerging role in cancer. Nat Rev Cancer 2003; 3: 110-116.

[13] Arai H, Hori S, Aramori I, Ohkubo H, Nakanishi S. Cloning and expression of a cDNA encoding an endothelin receptor. Nature 1990; 348: 730-732.

[14] Inoue A, Yanagisawa M, Kimura S, Kasuya Y, Miyauchi T, Goto K, Masaki T. The human endothelin family: three structurally and pharmacologically distinct isopeptides predicted by three separate genes. Proc Natl Acad Sci U S A 1989; 86: 2863-2867.

[15] Sakurai T, Yanagisawa M, Takuwa Y, Miyazaki H, Kimura S, Goto K, Masaki T. Cloning of a cDNA encoding a non-isopeptide-selective subtype of the endothelin receptor. Nature 1990; 348: 732-735.

[16] Spinella F, Rosano L, Di Castro V, Natali PG, Bagnato A. Endothelin-1 induces vascular endothelial growth factor by increasing hypoxia-inducible factor-1alpha in ovarian carcinoma cells. J Biol Chem 2002; 277: 27850-27855.

[17] Donckier JE, Mertens-Strijthagen J, Flamion B. Role of the endothelin axis in the proliferation of human thyroid cancer cells. Clin Endocrinol 2007; 67: 552-556.

[18] Donckier JE, Michel L, Delos M, Havaux X, Van Beneden R. Interrelated overexpression of endothelial and inducible nitric oxide synthases, endothelin-1 and angiogenic factors in human papillary thyroid carcinoma. Clin Endocrinol 2006; 64: 703-710.

[19] Donckier JE, Michel L, Van Beneden R, Delos M, Havaux X. Increased expression of endothelin-1 and its mitogenic receptor ETA in human papillary thyroid carcinoma. Clin Endocrinol 2003; 59: 354-360.

[20] Höltke C, Law MP, Wagner S, Kopka K, Faust A, Breyholz HJ, Schober O, Bremer C, Riemann B, Schäfers M. PET-compatible endothelin receptor radioligands: Synthesis and first in vitro and in vivo studies. Bioorg Med Chem 2009; 17: 7197-7208.

[21] Michel K, Buther K, Law MP, Wagner S, Schober O, Hermann S, Schafers M, Riemann B, Holtke C, Kopka K. Development and Evaluation of Endothelin-A Receptor (Radio)Ligands for Positron Emission Tomography. J Med Chem 2011; 54: 939-948.

[22] Maschauer S, Einsiedel J, Haubner R, Hocke C, Ocker M, Hübner H, Kuwert T, Gmeiner P, Prante O. Labeling and Glycosylation of Peptides Using Click Chemistry: A General Approach to 18F-Glycopeptides as Effective Imaging Probes for Positron Emission Tomography. Angew Chem Int Ed 2010; 49: 976-979.

[23] Maschauer S, Prante O. A series of 2-O-trifluoromethylsulfonyl-D-mannopyranosides as precursors for concomitant 18F-labeling and glycosylation by click chemistry. Carbohydr Res 2009; 344: 753-761.

[24] Cheng Y, Prusoff WH. Relationship between the inhibition constant (K1) and the concentration of inhibitor which causes 50 per cent inhibition (I50) of an enzymatic reaction. Biochem Pharmacol 1973; 22: 3099-3108.

[25] Bradford MM. A rapid and sensitive method for the quantitation of microgram quantities of protein utilizing the principle of protein-dye binding. Anal Biochem 1976; 72: 248-254.

[26] Alexanderson E, Garcia-Rojas L, Jimenez M, Jacome R, Calleja R, Martinez A, Ochoa JM, Meave A, Alexanderson G. Effect of ezetimibe-simvastatine over endothelial dysfunction in dyslipidemic patients: assessment by 13N-ammonia positron emission tomography. J Nucl Cardiol 2010; 17: 1015-1022.

[27] Reynolds EE, Keiser JA, Haleen SJ, Walker DM, Olszewski B, Schroeder RL, Taylor DG, Hwang O, Welch KM, Flynn MA, Thompson DM, Edmunds JJ, Barryman KA, Plummer M, Cheng XM, Patt WC, Doherty AM. Pharmacological characterization of PD 156707, an orally active ETA receptor antagonist. J Pharmacol Exp Ther 1995; 273: 1410-1417.